

# Experimental evaluation of the in-plane behaviour of masonry wall infilled RC frames

Tomomi Suzuki<sup>1</sup> · Ho Choi<sup>2</sup> · Yasushi Sanada<sup>1</sup> ·  
Yoshiaki Nakano<sup>2</sup> · Kazuto Matsukawa<sup>2</sup> · Devjyoti Paul<sup>3</sup> ·  
Polat Gülkan<sup>4</sup> · Baris Binici<sup>5</sup>

Received: 18 October 2016 / Accepted: 9 April 2017 / Published online: 19 April 2017  
© Springer Science+Business Media Dordrecht 2017

**Abstract** This study focuses on the in-plane behaviour of unreinforced masonry (URM) infill walls installed in reinforced concrete (RC) frames. Five 1/4-scale model frames were designed based on a prototype RC building with URM infill walls in Turkey. The experimental parameters were the layout of the URM infill (its presence or absence), number of spans (single or double), number of stories (single or double), and stacking pattern of the URM infill (horizontal or vertical). Static cyclic loading tests were conducted to investigate the lateral force resisting mechanisms in the in-plane direction, which were evaluated based on the strain data measured on blocks forming the infill walls. The results indicated the following: (1) The vertically stacked infill did not form a typical diagonal compressive strut and showed lower seismic performance than the horizontally stacked infill. (2) For the specimens with horizontally stacked infill, the one-story, two-bay specimen formed a diagonal compressive strut in each infill wall similar to that formed in the one-story, one-bay specimen, whereas a steeper compressive strut through both stories appeared in the two-story, one-bay specimen. To verify the above strut mechanisms in the horizontally stacked infill, the compressive struts in the specimens were quantitatively identified based on strain data recorded on the infill. The identified compressive struts indicated that single strut models were applicable to multi-bay infilled frames; however, the stress transfer across floors should be considered in multi-story frames.

---

✉ Ho Choi  
choiho@iis.u-tokyo.ac.jp

<sup>1</sup> Graduate School of Engineering, Osaka University, Osaka, Japan

<sup>2</sup> Institute of Industrial Science, The University of Tokyo, Tokyo, Japan

<sup>3</sup> Nippon Koei India Private Limited, New Delhi, India

<sup>4</sup> Civil Engineering Program, Middle East Technical University, Northern Cyprus Campus, Güzelyurt-Kalkanli, 99738 Mersin 10, Turkey

<sup>5</sup> Department of Civil Engineering, Middle East Technical University, Ankara, Turkey

**Keywords** Compressive strut · Masonry infill wall · RC moment-resisting frame · Seismic performance evaluation · Static cyclic loading test · Strain measurement

### List of symbols

$\Delta, R$	Lateral drift and drift angle at the uppermost beam in a specimen
$H$	Internal height of the wall
$Q_{My}, Q_{Sy}$	Shear force at flexural yielding and shear strength
${}^cM_c, {}^bM_c$	Cracking moment of the column and beam
${}^c\theta_c, {}^b\theta_c$	Rotation angle of the column and beam at the cracking moment
$f'_c$	Compressive strength of concrete
$Z$	Section modulus
$N, \sigma_0$	Axial force and axial stress
$b, D, d, h_0, l_0$	Width, depth, effective depth, clear height of the column, and clear length of the beam
$E, I$	Young's modulus and cross-sectional moment of inertia
${}^cM_y, {}^bM_y$	Flexural yield moment of the column and beam
${}^c\theta_y, {}^b\theta_y$	Rotation angle of the column and beam at the flexural yield moment
$g_1$	Ratio of the spacing between the centroids of the compressive and tensile longitudinal bars to the member depth
$a_t, p_t, p_w$	Gross area of tensile reinforcement and tensile and shear reinforcement ratios
$f_y, f_{wy}$	Yield stress of the longitudinal and shear reinforcements
$a$	Depth of the equivalent rectangular stress block
$j$	Distance between the centroids of the tensile and compressive stresses
${}^c\alpha_y, {}^b\alpha_y$	Reduction factor of the secant stiffness at yielding to the elastic stiffness of the column and beam
$n$	Ratio of the Young's modulus of the reinforcement to that of the concrete
$a', \eta_0$	Shear span and axial force ratio ( $=N/bDf'_c$ )
$MI/(Qd)$	Shear span-to-effective depth ratio ( $=h_0/(2d)$ )
$\varepsilon_j, \theta_j$	Principal compressive strain of the $j$ th block unit
$\varepsilon_{cm}$	Compressive strain at the maximum strength recorded during the prism test
$\theta$	Main diagonal strut angle
$\varepsilon_i$	Compressive strain of the $i$ th section
$\varepsilon_m$	Mean value of the compressive strain
$C_{y, i}$	Central axis distance of the $i$ th section
$C_y$	Equivalent central axis distance of the evaluated strut
$W_{e, i}$	Effective width of the $i$ th section
$W_{eq}$	Equivalent diagonal compressive strut width
$\sigma_m$	Equivalent compressive stress acting within the evaluated compressive strut
$t$	Wall thickness
$y_i$	Distance of each block in the $i$ th section from the reference line
$V_C$	Lateral shear strength of the URM infill wall

## 1 Introduction

Evidence to the contrary notwithstanding, unreinforced masonry (URM) infill walls are typically not considered as structural components in design codes. Thus, the seismic design of reinforced concrete (RC) moment-resisting frame buildings does not consider their structural performance. However, the effects of URM infill walls on the seismic performance of RC frames have been verified through surveys in the aftermath of past earthquakes as well as previous experimental studies (e.g., Hashemi and Mosalam 2007; Maidiawati et al. 2011). The primary difficulty associated with defining stable parameters that describe the structural action of infill walls is the variability of the masonry unit-mortar matrix due to the influences of workmanship, the snugness of the fit of the masonry with the RC enclosure and the bond between the masonry unit and the mortar paste. Empirical equations that work well with one combination of controlling parameters may perform poorly with other combinations.

Many researchers have studied the structural effects of infill walls and proposed evaluation methods based on the theory of compressive strut formation in URM infill walls. In these methods, evaluating the equivalent compressive strut width is one of the most important issues to assess the structural performance of infill walls; hence, several equations have been proposed to obtain the properties of the compressive strut and its width, as described below.

Holmes (1961) suggested that masonry infill in steel frames acted as a pin-jointed diagonal brace and that the strut width should be  $1/3$  of the diagonal length of the masonry infill. Stafford and Carter (1969) considered the interaction between the masonry infill and surrounding frame and suggested a definition of the equivalent strut width based on the relative stiffness between them. FEMA 306 (1998) recommended the use of the equivalent strut width based on empirical calculations provided by Mainstone (1971), which also considered the relative stiffness between the infill and boundary frame, to evaluate the stiffness and strength of URM infill. The strut widths theoretically or empirically evaluated by these studies were verified via comparisons between the experimental and simulation results in terms of the overall responses of the infilled frames. Recently, Turgay et al. (2014) evaluated the existing strut models employed by various codes based on approximately 50 frame test results. The accuracy of the existing strut models to estimate the stiffness of the test specimens was found to be low for use in design and assessment. This result demonstrated the need for accurate strut width models, preferably obtained directly from experimental data.

Jin et al. (2016) experimentally investigated the in-plane performance of two URM infilled in one-story, one-bay RC frames with a rigid or flexural upper boundary beam. The study proposed and verified an experimental evaluation method for the above-described width and relationship by using the test data of three-axis strain gauges attached to concrete block (CB) units. The significance of this evaluation method was to experimentally clarify how the compressive stresses were transferred within the URM infill walls.

In this study, the above-described experimental approach of Jin et al. (2016) is further extended to evaluate the performance of typical URM infilled RC frames in the Mediterranean Region by considering a wider range of parameters (e.g., different material characteristics, different specimen configurations, and different numbers of stories and bays) that can influence the response. The experimental program included one-story, two-bay and two-story, one-bay infilled frame specimens as well as one-story, one-bay specimens with or without URM infill. In particular, the experimental results reported herein

provide fundamental knowledge for numerical modelling of URM infill walls in multi-story, multi-bay RC buildings.

## 2 Experimental program

### 2.1 Prototype building and scaled specimens

A research project was initiated as a collaboration between European and Japanese universities under the JST (Japan Science and Technology Agency) Concert-Japan (Connecting and Coordinating European Research and Technology Development with Japan) project to improve the seismic performance of URM infill walls. A typical Turkish RC building with URM was selected as a reference building, and the 1/4-scale models were prepared and tested at the University of Tokyo. Figure 1 shows the outline of the reference building, which has five stories, with each story having a height of 3 m and plan dimensions of 23 m by 16 m. As shown in the figure, one span of the interior frame in the longitudinal direction in the first story was selected to design the prototype one-story, one-bay scaled model frame. In this study, however, five types of specimens were designed based on the prototype specimen considering the experimental parameters of the URM infill layout (presence or absence), number of spans (single or double), number of stories (single or double), and stacking pattern of URM infill (horizontal or vertical), as shown in Fig. 2: (a) one-story, one-bay bare frame (Specimen BF); (b) one-story, one-bay frame with horizontally stacked infill (Specimen 1S-1B); (c) one-story, one-bay frame with vertically stacked infill (Specimen 1S-1B-V); (d) one-story, two-bay with horizontally stacked infill (Specimen 1S-2B); and (e) two-story, one-bay with horizontally stacked infill (Specimen 2S-1B). In this study, a vertically stacked infill wall pattern, which is common in Turkey, was included to investigate the effect of the stacking pattern on the seismic performance.

### 2.2 Design of small-scale specimens

The 1/4-scale specimens were designed according to the following details (as shown for Specimen 1S-1B in Fig. 3) considering the similitude requirements.

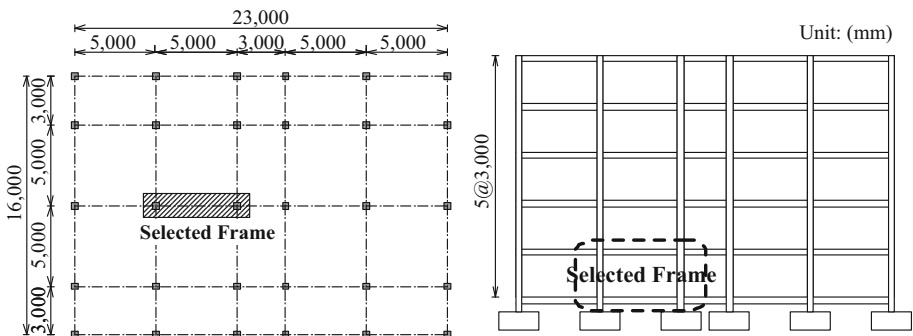


**Fig. 1** Outline of the reference building

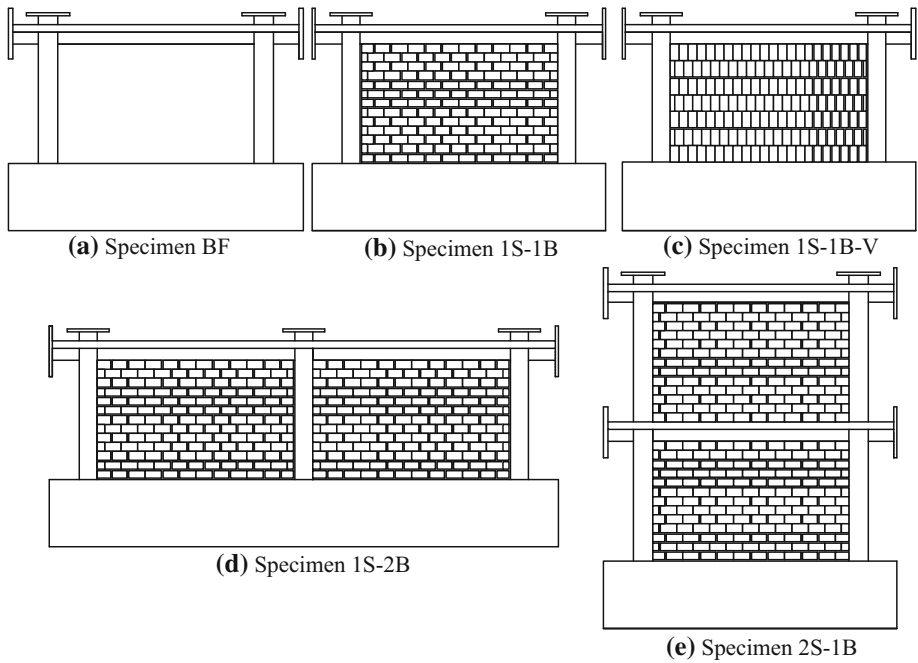


**Fig. 2** Elevations of the specimens

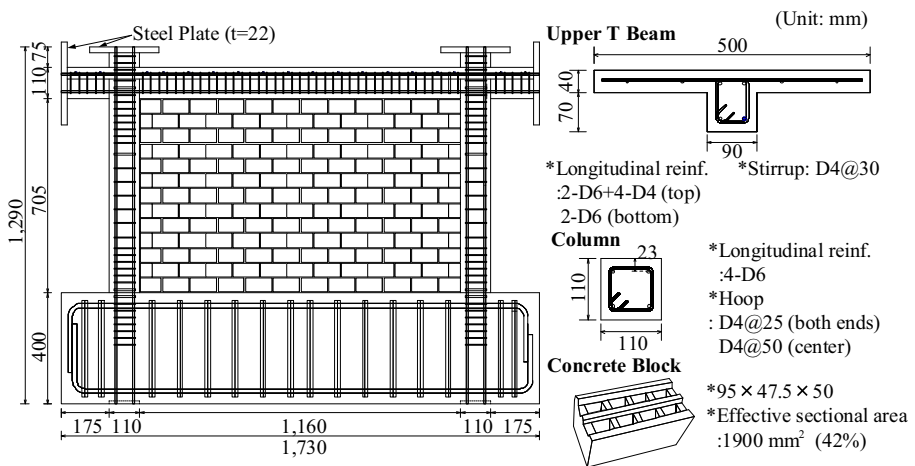


**Fig. 3** Details of specimen 1S-1B

### 2.2.1 Column and beam

Tables 1 and 2 compare the cross-sectional details, material properties and strengths of the column and beam for the reference building and specimen, respectively. As shown in the tables, the cross-sectional details of the beam/column were approximately 1/4 of those of

**Table 1** Main specifications of the full- and 1/4-scale columns

Main specifications	Full-scale	1/4-scale
Cross-sectional details		
Width and depth, $b$ and $D$ (mm)	450	110
Longitudinal reinforcement	8-D19	4-D6
Shear reinforcement	2-D13@100	2-D4@25
Clear height, $h_0$ (mm)	2800	705
Material properties		
Design compressive strength of concrete, $f'_c$ (N/mm <sup>2</sup> )	18	18
Tensile reinforcement ratio, $p_t$ (%)	0.42	0.47
Nominal yield stress of longitudinal reinforcement, $f_y$ (N/mm <sup>2</sup> )	295	295
Shear reinforcement ratio, $p_w$	0.008	0.009
Nominal yield stress of shear reinforcement, $f_{wy}$ (N/mm <sup>2</sup> )	295	295
Axial stress of column, $\sigma_0$ (N/mm <sup>2</sup> )	2.8	2.9
Strengths		
Shear force at flexural yielding, $Q_{My}$ (kN)	167.1	10.0
Shear strength, $Q_{Sy}$ (kN)	413.1	24.1
Shear-to-flexural strength ratio, $Q_{Sy}/Q_{My}$	2.47	2.41

**Table 2** Main specifications of the full- and 1/4-scale beams

Main specifications	Full-scale	1/4-scale
Cross-sectional details		
Top and bottom widths, $b_1$ and $b_2$ (mm)	2000/350	500/90
Depth, $D$ (mm)	450	110
Slab thickness, $t$ (mm)	150	40
Longitudinal reinforcement	2-D19 + 4-D13/2-D19 <sup>a</sup>	2-D6 + 4-D4/2-D6 <sup>a</sup>
Shear reinforcement	2-D13@100	2-D4@30
Clear length, $L$ (mm)	4550	1160
Material properties		
Design compressive strength of concrete, $f'_c$ (N/mm <sup>2</sup> )	18	18
Tensile reinforcement ratio, $p_t$ (%)	0.4/0.2 <sup>a</sup>	0.4/0.2 <sup>a</sup>
Nominal yield stress of longitudinal reinforcement, $f_y$ (N/mm <sup>2</sup> )	295	295
Shear reinforcement ratio, $p_w$	0.008	0.009
Nominal yield stress of the shear reinforcement, $f_{wy}$ (N/mm <sup>2</sup> )	295	295
Strengths		
Shear force at flexural yielding, $Q_{My}$ (kN)	96.1/58.5 <sup>a</sup>	5.9/3.5 <sup>a</sup>
Shear strength, $Q_{Sy}$ (kN)	422	26.0
Shear-to-flexural strength ratio, $Q_{Sy}/Q_{My}$	4.39/7.21 <sup>a</sup>	4.41/7.43 <sup>a</sup>

<sup>a</sup> Top value/bottom value

the reference building. The area ratios of the longitudinal and shear reinforcement to the beam/column cross-sectional area were designed to be approximately equal to those of the reference building. The column and upper beam had a T-shaped section, and the effective widths of the slabs were designed such that the shear-to-flexural strength ratios ( $Q_{Sy}/Q_{My}$ ) were equivalent to those of the reference building.  $Q_{My}$  and  $Q_{Sy}$  were calculated using Eqs. (1) and (2), respectively, as is commonly done in design practice in Japan (Architectural Institute of Japan (AIJ) 2016).

The experimental results for the concrete and steel bars are shown in Tables 3 and 4, respectively, where each value represents the mean value of 3 samples. Although the design compressive strength of concrete was 18 N/mm<sup>2</sup>, the value from the test cylinders exceeded this value, as shown in Table 3. The yield stresses of the reinforcement had values that were 35% higher than the nominal yield stress of 295 N/mm<sup>2</sup>, as shown in Table 4.

$$Q_{My} = 2M_y/h_0 = \left\{ g_1 a_t f_y D + 0.5ND \left( 1 - \frac{N}{bDf'_c} \right) \right\} / h_0 \tag{1}$$

$$Q_{Sy} = \left\{ \frac{0.068p_t^{0.23}(18 + f'_c)}{M/(Q \cdot d) + 0.12} + 0.85\sqrt{p_w \cdot f_{wy}} + 0.1\sigma_0 \right\} \cdot b \cdot j \tag{2}$$

where  $Q_{My}$  and  $Q_{Sy}$  are the shear force at flexural yielding and shear strength, respectively;  $M_y$  is the flexural yield moment;  $g_1$  is the ratio of spacing between the centroids of the compressive and tensile longitudinal bars to the beam/column depth;  $h_0$ ,  $b$ ,  $D$ , and  $d$  are the clear height, width, depth, and effective depth of the beam/column, respectively;  $a_t$  and  $p_t$  are the gross area of tensile reinforcements and the tensile reinforcement ratio, respectively;  $f_y$  is the yield stress of the longitudinal reinforcement;  $N$  is the applied axial force;  $f'_c$  is the compressive strength of concrete;  $M/(Qd)$  is the shear span-to-effective depth ratio ( $=h_0/(2d)$ );  $p_w$  is the shear reinforcement ratio;  $f_{wy}$  is the yield stress of the shear reinforcement;  $\sigma_0$  is the axial stress ( $=N/(bD)$ ); and  $j$  is the distance between the centroids of the tensile and compressive stresses ( $\approx 7d/8$ ).

### 2.2.2 Masonry unit

Table 5 shows the cross-sectional details and experimental results of the full- and small-scale masonry units. The masonry unit employed in the tests was also scaled by 1/4, as shown in Fig. 3 and Table 5. In this study, the CB unit was employed instead of the hollow clay brick that is generally used in Turkey. However, the cement-to-sand ratio was adjusted such that the strength and stiffness of the three-layered CB prism specimens were similar to those of the full-scale hollow clay brick, as shown in Table 5. Further details can be found in Gülkan et al. (2015).

**Table 3** Material test results of the concrete

Compressive strength $f'_c$ (N/mm <sup>2</sup> )	Young's modulus $E_c$ (N/mm <sup>2</sup> )
24.1	$2.1 \times 10^4$

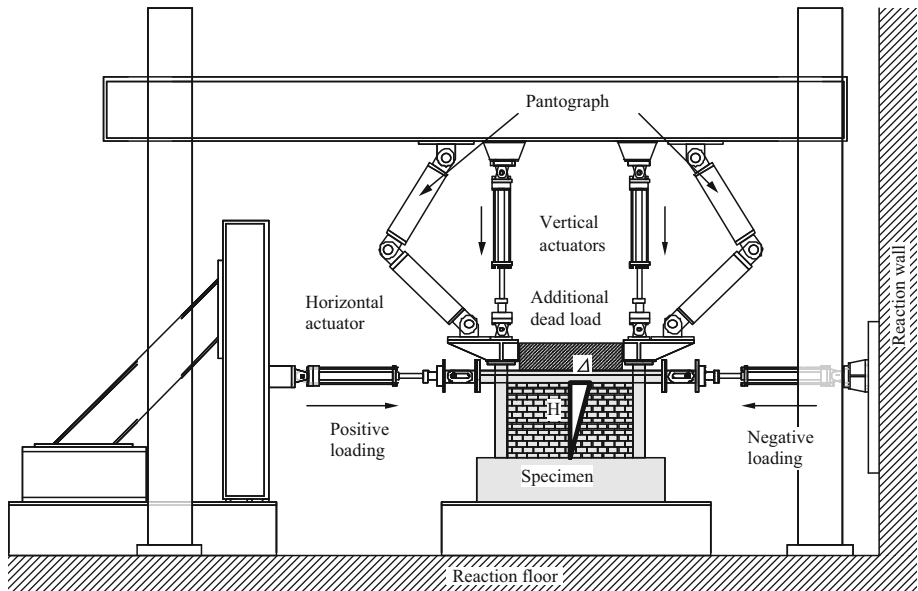
**Table 4** Material test results of the steel bars

	Yield stress $f_y$ (N/mm <sup>2</sup> )	Young's modulus $E_s$ (N/mm <sup>2</sup> )
D4	401	$2.1 \times 10^5$
D6	407	$2.0 \times 10^5$

**Table 5** Main specifications of the full- and 1/4-scale masonry units

Main specifications	Full-scale	1/4-scale
Cross-sectional details		
Width $\times$ depth $\times$ height (mm)	390 $\times$ 190 $\times$ 190	95 $\times$ 47.5 $\times$ 50
Hollow ratio to gross sectional area (%)	55	58
Material test results of masonry prisms		
Compressive strength, $f_m$ (N/mm <sup>2</sup> )	9.7/3.7 <sup>a</sup>	8.4/3.6 <sup>a</sup>
Young's modulus, $E_m$ ( $\times 10^3$ N/mm <sup>2</sup> )	4.0/3.9 <sup>a</sup>	4.6/4.8 <sup>a</sup>
Strain at the compressive strength, $\varepsilon_{cm}$ ( $\mu$ )	–/–	1168/313 <sup>a</sup>

<sup>a</sup> Horizontal stacking/vertical stacking

**Fig. 4** Loading system for specimen 1S-1B

### 2.3 Test methods

A loading system for the static cyclic in-plane loading tests is shown in Fig. 4. Lateral loads in the positive and negative directions were applied to the left and right ends of the uppermost beam with hydraulic actuators, respectively; for Specimen 2S-1B, the horizontal



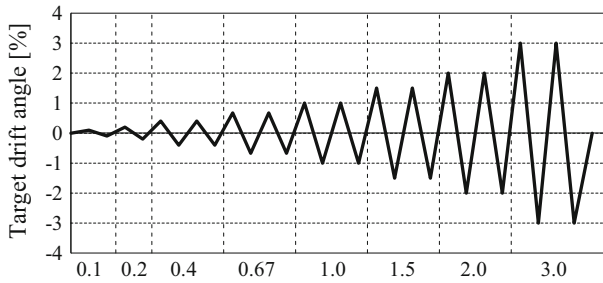


**Fig. 5** Lateral loading protocol

actuators were attached only on both ends of the top beam. Vertical actuators were installed to apply a constant axial load of 35 kN ( $2.9 \text{ N/mm}^2$ ) on the top of each column, and a distributed load of 5.9 kN/m (in total 7.5 kN) was also applied considering a design dead load on each slab. Two pantographs were used to eliminate the out-of-plane response during the tests. Figure 5 shows a lateral loading protocol that was controlled by a drift angle  $R$ , defined as a lateral drift  $\Delta$  at the centre of the uppermost beam divided by the height from the bottom of the specimen,  $H$ , as shown in Fig. 4.

A key objective of the tests was to measure the strain data on each block in the specimens. However, it was impossible to measure strains of all blocks for Specimens 1S-2B and 2S-1B because of limitations in the measurement equipment; therefore, approximately one-half of the blocks was selected to evaluate the strut mechanisms in the positive loading direction according to the method proposed in the previous study (Jin et al. 2016), as illustrated below. Figure 6 shows the strain gauge arrangements for all specimens with URM infill walls.

### 3 Experimental results

#### 3.1 Failure patterns and lateral force-drift angle relationships

Figures 7 and 8 show the crack patterns after the cycle of  $R = 3.0\%$  rad. and the lateral force-drift angle relationships of all specimens, respectively. The behaviour of each specimen to failure is summarized below.

##### 3.1.1 Specimen BF

Flexural cracks began to be observed at the column ends from a small drift angle,  $R$ , of 0.1% rad. and at the beam ends at  $R = 0.4\%$  rad. Flexural plastic hinges occurred at the bottoms of both columns during the cycle to  $R = 1.0\%$  rad. Shear cracks began to be observed at the beam-column joints in the same cycle. The beam yielded in flexure at the end framing into the tensile column at  $R = 1.5\%$  rad. In the following cycle to  $R = 2.0\%$  rad., flexural yielding occurred at the top of the compressive column and the adjoining beam end at the same loading step; thus, a yield mechanism was formed in the specimen. In addition, this specimen did not show significant strength deterioration until the final loading cycle. The maximum lateral strengths were 19.0 kN at  $R = 1.5\%$  rad and  $-21.0 \text{ kN}$  at  $R = -1.5\%$  rad. in the positive and negative loadings, respectively.

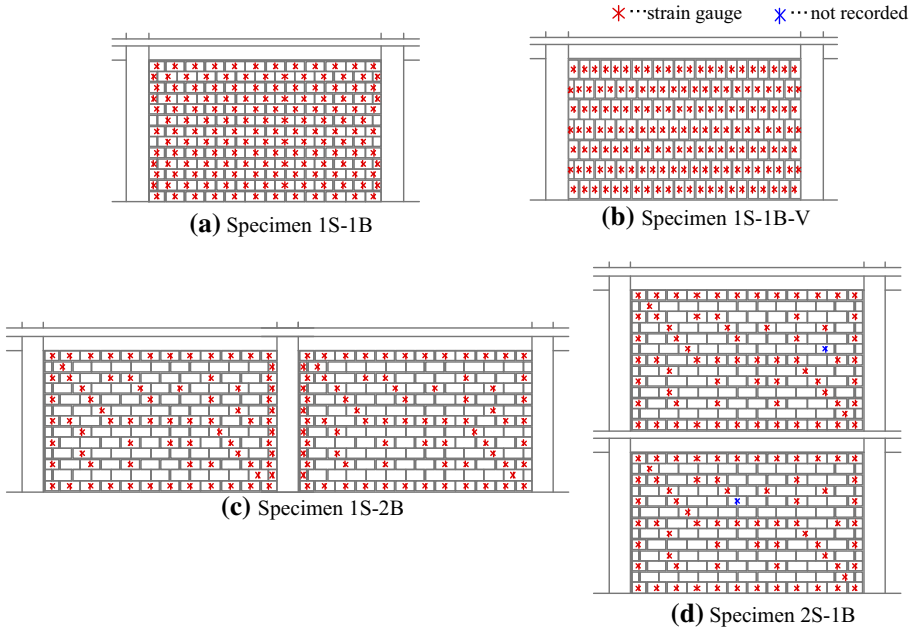


**Fig. 6** Strain gauge arrangements of masonry infill

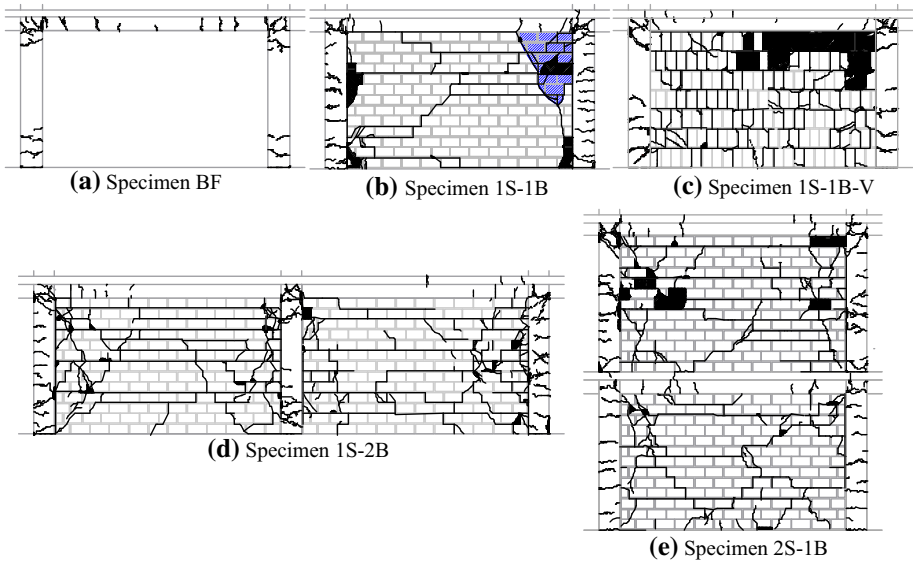


**Fig. 7** Final crack patterns after the cycle to  $R = 3.0\%$

Figure 8a compares the nonlinear monotonic analysis result of this specimen with the test results. In this analysis, the performance curves of a column and beam were replaced by a trilinear function with flexural cracking and yielding points, as shown in Fig. 9, based on Eqs. (3)–(12) for a practical design (Architectural Institute of Japan (AIJ) 2016;

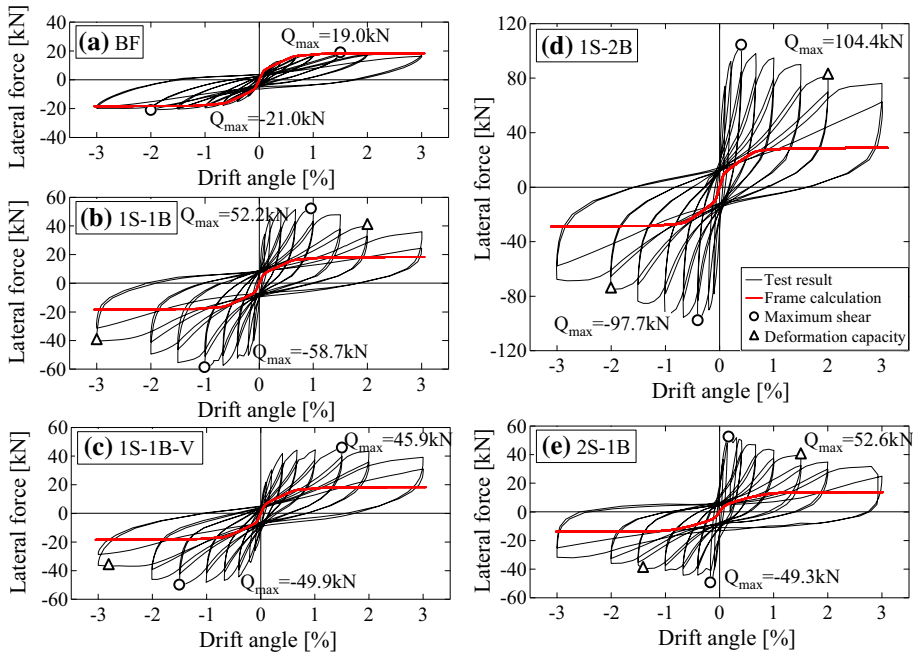


**Fig. 8** Lateral force-drift angle relationships from the experiments

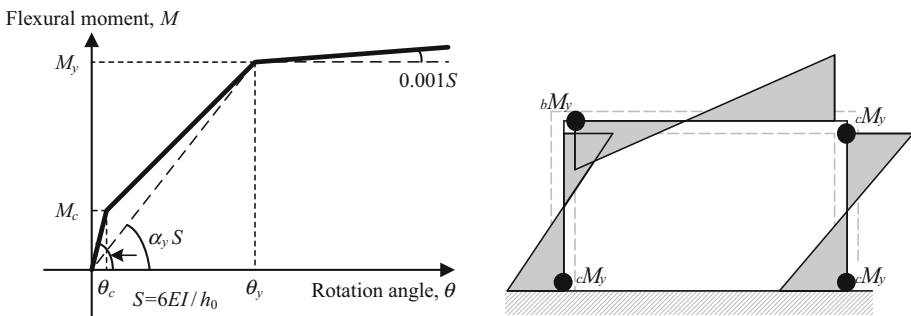


**Fig. 9** Modelling of each member and the resultant yield mechanism of specimen BF

American Concrete Institute (ACI) 2014). The cracking moment  $M_c$  and rotation  $\theta_c$  of a column and beam were evaluated using Eqs. (3)–(6), and the yielding moment  $M_y$  and rotation  $\theta_y$  of a column and beam were evaluated using Eqs. (7) through (10), which are based on general bending theories. However, in the case of the columns, varying axial forces were considered for  $N$  in Eq. (7) as a result of the shear force produced in the beam. The value of  $\alpha_y$  given by Eqs. (11) and (12) provides a secant stiffness at the yielding moment, as shown in Fig. 9. The post-yield stiffness was assumed to be 0.1% of the elastic stiffness.

Figure 9 shows the flexural plastic hinge formation of this specimen that was evaluated based on Eqs. (7) and (8) and that corresponds well with the aforementioned test results.

Furthermore, the analytical performance curve was consistent with the test results, as shown in Fig. 8a. The analytical results for RC frames in the other specimens are plotted in Fig. 8b through d.

$${}_cM_c = 0.56\sqrt{f'_c} \cdot Z + \frac{ND}{6} \quad (3)$$

$${}_bM_c = 0.56\sqrt{f'_c} \cdot Z \quad (4)$$

$${}_c\theta_c = \frac{h_0}{6EI} \cdot {}_cM_c \quad (5)$$

$${}_b\theta_c = \frac{l_0}{6EI} \cdot {}_bM_c \quad (6)$$

$${}_cM_y = g_1 \cdot a_t \cdot f_y \cdot D + 0.5 \cdot N \cdot D \cdot \left(1 - \frac{N}{b \cdot D \cdot f'_c}\right) \quad (7)$$

$${}_bM_y = 0.85 \cdot f'_c \cdot a \cdot b \cdot j \quad (8)$$

$${}_c\theta_y = \frac{h_0}{6EI} \cdot \frac{1}{{}_c\alpha_y} \cdot {}_cM_y \quad (9)$$

$${}_b\theta_y = \frac{l_0}{6EI} \cdot \frac{1}{{}_b\alpha_y} \cdot {}_bM_y \quad (10)$$

$${}_c\alpha_y = (0.043 + 1.64 \cdot n \cdot p_t + 0.043 \cdot a'/D + 0.33 \cdot \eta_0) \cdot \left(\frac{d}{D}\right)^2 \quad (11)$$

$${}_b\alpha_y = (0.043 + 1.64 \cdot n \cdot p_t + 0.043 \cdot a'/D) \cdot \left(\frac{d}{D}\right)^2 \quad (12)$$

where  ${}_cM_c$  and  ${}_bM_c$  are the cracking moment of the column and beam, respectively;  ${}_c\theta_c$  and  ${}_b\theta_c$  are the rotation angle of the column and beam at the cracking moment, respectively;  $Z$  is the section modulus;  $N$  is the axial force;  $l_0$  is the clear length of the beam;  $E$  is the Young's modulus of concrete;  $I$  is the cross-sectional moment of inertia;  ${}_cM_y$  and  ${}_bM_y$  are the flexural yield moment of the column and beam, respectively;  ${}_c\theta_y$  and  ${}_b\theta_y$  are the rotation angle of the column and beam at the yield moment, respectively;  $a$  is the depth of equivalent rectangular stress block;  ${}_c\alpha_y$  and  ${}_b\alpha_y$  are the reduction factors of secant stiffness at the yield moment to the elastic stiffness of the column and beam, respectively;  $n$  is the ratio of the Young's modulus of the reinforcement to that of the concrete;  $a'$  is the shear span; and  $\eta_0$  is the axial force ratio ( $=N/bDf'_c$ ).

### 3.1.2 Specimen IS-1B

Focusing on the infill wall, horizontal cracks and stair step cracks occurred on the wall from a small drift,  $R$ , of 0.1% rad.; the majority of these cracks were observed on the joint mortar. These cracks developed until the maximum strengths were recorded and widely opened beyond drifts at the peak strengths. In addition, the sliding behaviour was observed along the horizontal crack between the fourth and fifth layers from the top, resulting in

separation of the right-top corner units from the wall (hatched area in Fig. 7b) showing rocking behaviour. Crushing and spalling off of the blocks caused significant strength reductions of the specimen.

The boundary frame exhibited a different crack pattern compared to that of Specimen BF, as shown in Fig. 7. Horizontal cracks were observed not only at both column ends but also in the middle height of the columns, indicating that the infill wall formed a compression strut along the diagonal direction that applied the reactional tension to the top of the column on the tensile side.

The maximum strengths reached 52.2 kN and  $-58.7$  at  $R = 1.0\%$  rad. and  $-1.5\%$  rad., respectively, which were approximately 2.8 times those of Specimen BF. These improvements verified a high contribution of the infill to the overall strength. The deformation capacities, which were defined as a drift when the lateral resistance decreased to 80% of the maximum strength, were 2.0 and  $-3.0\%$  rad. in the positive and negative directions, respectively. These values were smaller than those of Specimen BF (over  $R = 3.0\%$ ) because of the punching shear forces applied to the column ends from the infill strut.

### 3.1.3 Specimen 1S-1B-V

In the case of vertically stacked blocks, additional cracks were observed on the joint mortar, even during the loading cycles to small drifts, with the appearance of stair-step patterns. Many blocks rotated and thus created gaps between adjacent blocks, which were observed beyond drifts at the peak strengths. Consequently, the initial stiffness and maximum strength were lower than those of Specimen 1S-1B with horizontally laid blocks. The maximum strengths were 45.9 and  $-49.9$  kN at the peak drifts in the cycle to 1.5% rad. This specimen did not degrade to the deformation capacity defined above under the positive loading.

### 3.1.4 Specimen 1S-2B

This specimen had the highest initial stiffness and maximum strength among the five specimens. Compared with Specimen 1S-1B, the maximum strength was approximately two times greater: 104.4 kN at  $R = 0.4\%$  rad. Many wide cracks were observed at both ends of the middle column because of the punching shear applied to the column ends by both sides of the infill walls. The crack patterns on both walls were similar to that of Specimen 1S-1B.

### 3.1.5 Specimen 2S-1B

The lateral loading for this specimen was controlled by an overall drift angle, which was obtained by a horizontal displacement at the second-floor beam divided by its height from the bottom, as noted in Sect. 2.3.

Few cracks were observed on the second-story infill wall until the lateral force reached the maximum strength. At that point, diagonal cracks in the wall and shear cracks in the tensile column in the second story triggered a decrease in the lateral resistance of the specimen. Consequently, the specimen formed a story collapse mechanism in the second story.

The initial stiffness of this specimen was higher than that of Specimen 1S-1B because the deformation of middle beam was restrained by the upper and lower walls. As a result, the maximum strengths were recorded at relatively smaller angles of 0.17 and  $-0.4\%$ , which were 52.6 and  $-49.3$  kN in the positive and negative loading, respectively.

### 3.2 Principal compressive strain distributions of the infill walls in the specimens

The strains of the CBs were measured by using three-axis strain gauges as arranged in Fig. 6, and the maximum and minimum principal strains of the blocks were analysed based on the general theory (Gere and Timoshenko 1997). Figure 10 shows the principal compressive strains of the infill blocks at the maximum strength of each specimen in the positive direction. Each arrow in the figure denotes a vector of each principal compressive strain.

In Specimen 1S-1B, the compressive strains of CB units implied the formation of a diagonal compressive strut in the URM infill; however, the compressive strains measured on the separated piece of the infill (refer to Fig. 7b) were also high because the rocking behaviour discussed in Sect. 3.1.2 was constrained by the right column and the top beam.

In contrast, Specimen 1S-1B-V did not show a clear diagonal strut. CB units with high strains were generally scattered, whereas lower strains were recorded in the central units in the wall. The rocking behaviour of each independent unit was clearly observed, particularly in the central part of the wall, which might have affected such strain distributions.

Although the strain measurements could not be performed for all blocks in Specimens 1S-2B and 2S-1B, in the case of Specimen 1S-2B, most principal compressive strains of

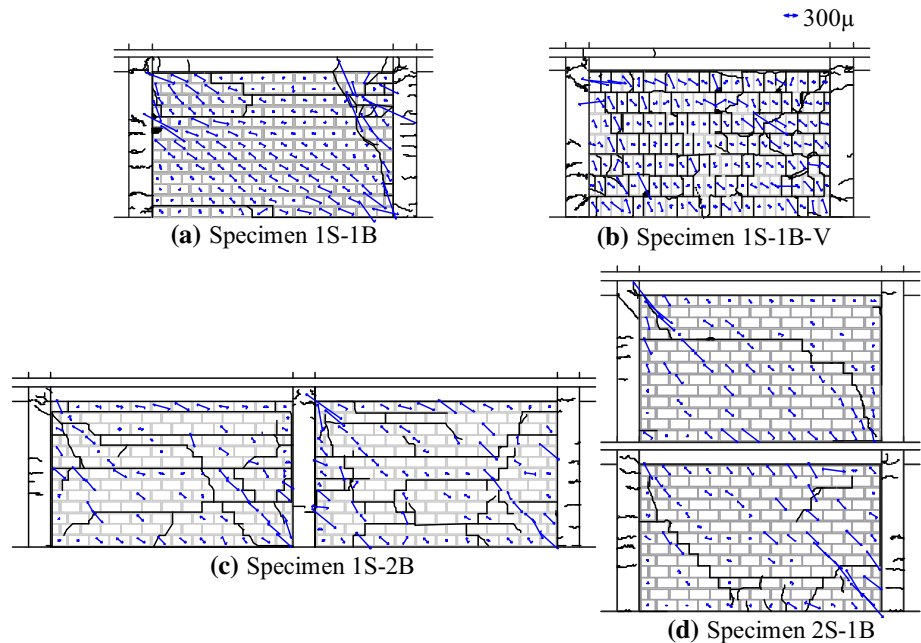


**Fig. 10** Principal compressive strain drawings at the maximum strengths in the positive direction

CB units were found in the diagonal direction. This result indicated that a diagonal compressive strut was formed in each wall.

Focusing on Specimen 2S-1B, higher strains were observed on CB units along the diagonal direction between the left-top corner in the second-story infill and the right-bottom corner in the first-story infill, implying that a compression strut might be formed through both stories.

The above observation results of Specimens 1S-2B and 2S-1B will be discussed in greater detail below.

## 4 Experimental identification of the single strut mechanism for the infill walls

The specimens appeared to form single or multiple diagonal struts in the infill walls, except for Specimen 1S-1B-V with the vertically stacked infill, as noted in the experimental results. Focusing on Specimens 1S-1B, 1S-2B, and 2S-1B with the horizontally stacked infill, the lateral force-resisting mechanisms of the infill walls were investigated based on the method to identify a single compression strut by Jin et al. (2016). The method presents a scheme to identify the strut parameters including the main angle, average compressive strain, and equivalent width using the experimental strain data (in Fig. 10), as summarized in the following.

### 4.1 Selection of effective CB units

The effective CB units are defined as those units before fracture (i.e., penetrated cracks) satisfying Eqs. (13) and (14).

$$0^\circ < \theta_j < 90^\circ \quad (13)$$

$$\varepsilon_j < \varepsilon_{cm} \quad (14)$$

where  $\theta_j$  is the principal compressive strain angle with respect to the horizontal line of the  $j$ th unit in all CB units;  $\varepsilon_j$  is the principal compressive strain of the  $j$ th unit; and  $\varepsilon_{cm}$  is the compressive strain at the maximum strength from the material test.

### 4.2 Main diagonal strut angle $\theta$

The main diagonal strut angle  $\theta$  was then estimated from the principal compressive strains and angles of the effective CB units defined in Sect. 4.1. In this study, the average of the principal compressive angles weighted with the strains was employed to calculate the main diagonal strut angle  $\theta$ , as shown in Eq. (15).

$$\theta = \frac{\sum_{j=1}^l (\varepsilon_j \times \theta_j)}{\sum_{j=1}^l \varepsilon_j} \quad (15)$$

where  $l$  is the number of the effective CB units;  $\varepsilon_j$  is the principal compressive strain of the  $j$ th unit in all effective CB units; and  $\theta_j$  is the principal compressive strain angle of the  $j$ th unit.

### 4.3 Division of the wall panel

The wall was divided by inclined sections to calculate the equivalent strut described in the following Sect. 4.6, as shown in Fig. 11. These sections were perpendicular to a reference line with the main diagonal strut angle  $\theta$  from the horizontal axis obtained as above and were equally spaced, with a maximum spacing containing at least one CB unit of each horizontal layer. The wall was consequently divided into 18 sections, as shown in Fig. 11.

### 4.4 Mean strain $\epsilon_m$ of the equivalent diagonal strut

The mean value  $\epsilon_i$  of the principal compressive strains of the CB units included in the  $i$ th section ( $i = 1-18$ ) was calculated first. Subsequently, the mean strain  $\epsilon_m$  for the strut was calculated using Eq. (16).

$$\epsilon_m = \sum_{i=1}^n \epsilon_i / n \quad (n = 18 \text{ herein}). \tag{16}$$

### 4.5 Central axis distance $C_y$ of the equivalent diagonal strut

The central axis distance from reference line  $C_y$  of the equivalent diagonal strut was calculated using the centroid distance  $C_{y,i}$  of each section.  $C_{y,i}$  and  $C_y$  were calculated using Eqs. (17) and (18), respectively.

$$C_{y,i} = \sum_{j=1}^m (\epsilon_j \times y_j) / \sum_{j=1}^m \epsilon_j \tag{17}$$

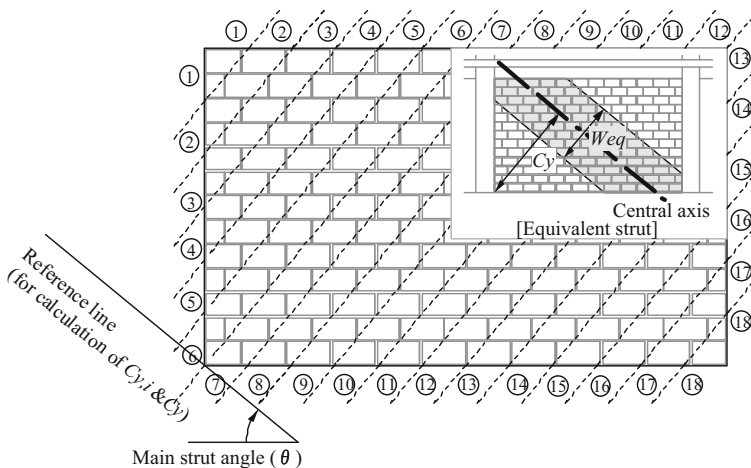


**Fig. 11** Main strut angle, central axis and equivalent strut width



$$C_y = \frac{\sum_{i=1}^n (\varepsilon_i \times C_{y,i})}{\sum_{i=1}^n \varepsilon_i} \quad (n = 18) \tag{18}$$

where  $y_j$  is the distance of each block with  $0^\circ < \theta_j < 90^\circ$  in the  $i$ th section from the reference line (shown in Fig. 11) and  $m$  is the number of blocks with  $0^\circ < \theta_j < 90^\circ$  in each section.

### 4.6 Equivalent diagonal strut width $W_{eq}$

The effective width  $W_{e,i}$  of strut at every section  $i$  was calculated first.  $W_{e,i}$  was defined as the outermost distance between the effective CB units, as shown in Fig. 12. The equivalent diagonal strut width  $W_{eq}$  was calculated by Eq. (19). In this study, the average of  $W_{e,i}$  weighted with the mean value of principal compressive strain  $\varepsilon_i$  was employed as the equivalent diagonal strut width  $W_{eq}$ .

$$W_{eq} = \frac{\sum_{i=1}^n (\varepsilon_i \times W_{e,i})}{\sum_{i=1}^n \varepsilon_i} \quad (n = 18). \tag{19}$$

As for Specimens 1S-2B and 2S-1B, it was impossible to measure strain data on all blocks because of the limitations in the measurement equipment, as noted in Sect. 2.3; therefore, approximately half the number of blocks were selected such that each section included blocks located at both ends and the spacing between blocks with strain gauges were as uniformly distributed as possible under the positive loading, as shown in Fig. 12.

### 4.7 Shear resistance of an URM infill wall

The shear resistance of an URM infill wall  $V_c$  was calculated from Eq. (20) based on the properties of the equivalent diagonal strut. In this equation,  $\sigma_m$  is the principal compressive stress corresponding to the mean principal compressive strain  $\varepsilon_m$  of the equivalent diagonal

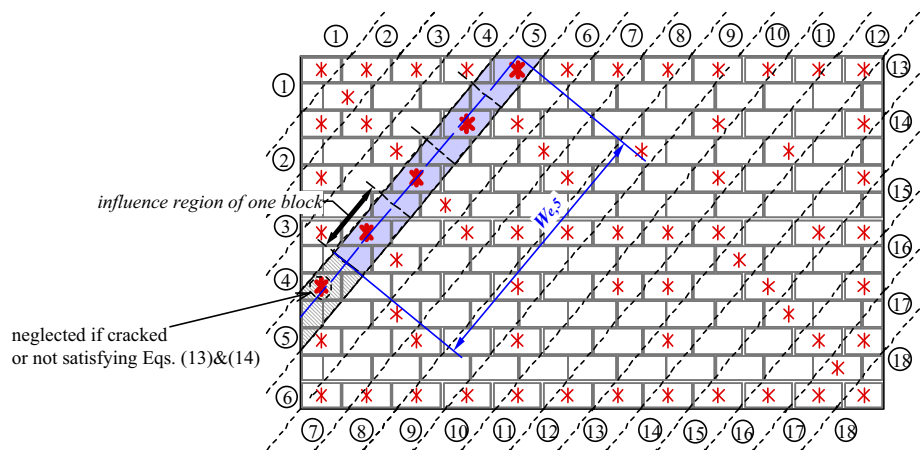
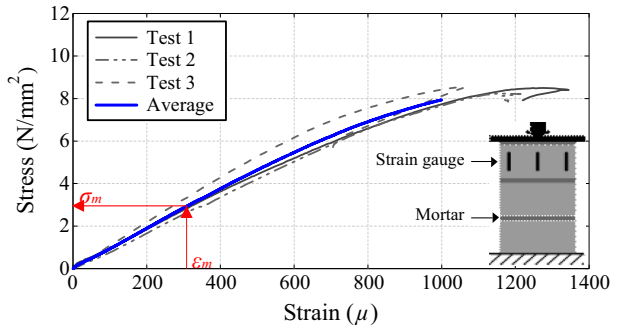


**Fig. 12** Definition of  $W_{e,i}$  for Specimens 1S-2B and 2S-1B

**Fig. 13**  $\sigma_m$ - $\epsilon_m$  relationships of the CB three-layered prism tests



strut. In this study,  $\sigma_m$  was obtained from the stress ( $\sigma_m$ )-strain ( $\epsilon_m$ ) relationship of the three-layered prism tests, as shown in Fig. 13.

$$V_c = W_{eq} \cdot \cos \theta \cdot \sigma_m \cdot t \tag{20}$$

where  $W_{eq}$  is the equivalent strut width;  $\theta$  is the main strut angle;  $\sigma_m$  is the stress corresponding to the equivalent strut's principal compressive strain  $\epsilon_m$  based on the three-layered prism tests; and  $t$  is the thickness of the wall (47.5 mm).

## 5 Discussion of the lateral resistances of the infill walls

### 5.1 Verification of the effectiveness of the strain gauge arrangements

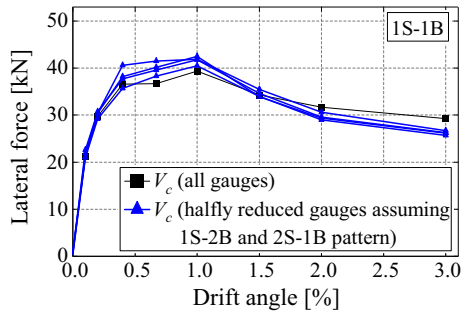
As noted above, the strain gauges of Specimens 1S-2B and 2S-1B were sparse, and the effects of the strain gauge arrangements on the compressive strut identification and the shear resistance evaluation were first verified in the following by comparing two results; i.e. (1) those using all of the strain data and (2) those using half of the data of Specimen 1S-1B, which had a strain gauge on all CB units. In case (2), the strain data were from selected

**Table 6** Comparison of calculated parameters based on different strain gauge arrangements

Gauge arrangements	$\theta$ (°)	$W_{eq}$ (mm)	$C_y$ (mm)	$\epsilon_m$ (μ)	$\sigma_m$ (N/mm <sup>2</sup> )	$V_c$ (kN)
All gauge						
1S-1B	39.0	406	537	279	2.66	39.8
Selected pattern						
1S-2B						
Left infill	39.4	401	556	291	2.85	41.9
Right infill	39.0	402	525	286	2.73	40.5
2S-1B						
Top infill	39.0	404	535	299	2.85	42.5
Bottom infill	39.0	404	529	295	2.81	41.8

At  $R = + 1.0\%$  of Specimen 1S-1B

**Fig. 14** Comparison of the lateral force-drift angle relationships estimated for the infill wall in 1S-1B based on different strain gauge arrangements



gauges located at the same positions as each gauge layout adopted for 1S-2B (left/right wall) and 2S-1B (top/bottom wall).

As shown in Table 6, the evaluated parameters based on four patterns of strain gauge arrangements showed good agreement with those from all strain gauges in Specimen 1S-1B. Furthermore, the shear forces carried by the infill wall of Specimen 1S-1B were evaluated at every peak drift angle according to Eq. (20). The evaluated shear force-drift angle relationships were successfully reproduced, even from the half number of gauge data, as shown in Fig. 14.

### 5.2 Experimental identification of equivalent diagonal strut

Table 7 and Fig. 15 show the evaluated parameters for the equivalent diagonal strut at the maximum strength of each specimen using the method described above.

The equivalent diagonal strut widths of the walls using the proposed method were 387–617 mm, as shown in Table 7 and Fig. 15, whereas the equivalent strut width calculated using FEMA (1998) was 217 mm. This value is considerably smaller than those obtained from the proposed method, resulting in underestimated experimental stiffness and maximum wall strength.

The equivalent compressive struts of all specimens had higher main strut angles  $\theta$  than the diagonal angle of the infill ( $=32.9^\circ$ ). These results corresponded to the evaluation result of the specimen with a flexible beam reported by Jin et al. (2016).

**Table 7** Evaluated parameters of equivalent diagonal struts

Specimen	$\theta$ ( $^\circ$ )	$W_{eq}$ (mm)	$C_y$ (mm)	$\varepsilon_m$ ( $\mu$ )	$\sigma_m$ (N/mm <sup>2</sup> )	$V_c$ (kN)
1S-1B	39.0	406	537	279	2.66	39.8
1S-2B						
Left infill	41.9	448	603	233	2.22	35.1
Right infill	43.3	468	612	293	2.79	45.1
2S-1B						
Top infill	48.3	617	656	192	1.82	35.4
Bottom infill	44.6	387	769	291	2.77	36.3

At the maximum strength of each specimen

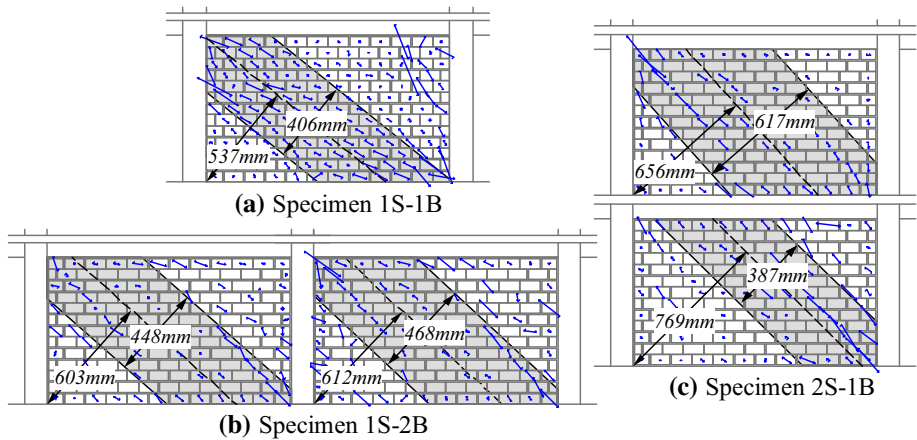


**Fig. 15** Sketches of the evaluated equivalent diagonal struts at the maximum strengths

A comparison of Figs. 10a and 15a for Specimen 1S-1B indicated that the identified strut was in good agreement with the area showing high strains. In the case of Specimen 1S-2B shown in Fig. 15b, the compressive struts at the maximum strength ( $R = 0.4\%$ ) were individually formed in both walls; thus, the summation of shear resistance  $V_c$  of both walls was approximately twice the infill resistance of Specimen 1S-1B, as observed in the tests. However, the main diagonal strut angle  $\theta$ , central axis distance  $C_y$  and equivalent diagonal strut width  $W_{eq}$  of Specimen 1S-2B were slightly larger than those of Specimen 1S-1B, possibly due to some CB units being neglected (at the right-top corner of the infill in Specimen 1S-1B, as shown in Fig. 7b) according to Eq. (13) or (14). The results of Specimen 1S-2B indicate that multi-bay walls can be modelled based on an equivalent single strut in each bay.

In contrast, in the case of Specimen 2S-1B shown in Fig. 15c, the equivalent compressive struts in both walls were formed in a different manner. In particular, compared to the other specimens, the central axis distance  $C_y$  was higher in the bottom wall, indicating that the compressive strut might be formed through both stories. The compressive strut identification applied herein assumed a single strut formation in each infill; it cannot identify multiple strut formations. In addition, considering the wider strut width in the second story, where the story collapse mechanism was formed in the experiment, Specimen 2S-1B might form multiple struts in the second story, as shown in Fig. 16. Moreover, such behaviour might be attributed to the loading scheme: the lateral loading was applied only to the top beam in the test, as noted in Sect. 2.3.

### 5.3 Verification of the identified compressive struts

Figure 17 compares the lateral force-drift angle relationships of Specimens 1S-1B, 1S-2B and 2S-1B between the experimental and estimated values, where both values were obtained from the applied loads and strain data. Namely, the estimated values were calculated as a summation of  $V_c$  using the experimental strain data and the performance curve of the RC frame evaluated in Fig. 8, and the experimental values were the test results shown in Fig. 8.

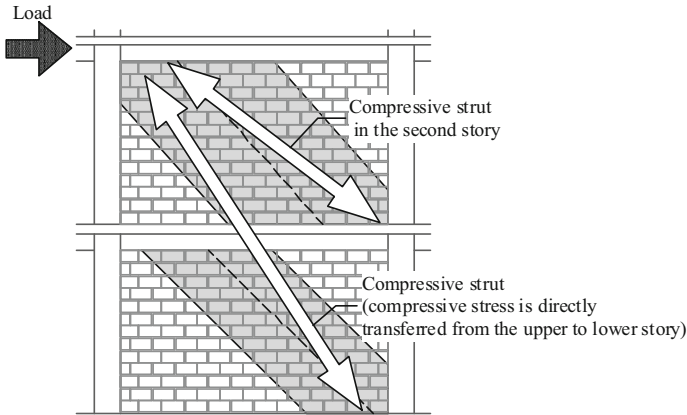


**Fig. 16** Possible multiple compressive strut formation in Specimen 2S-1B

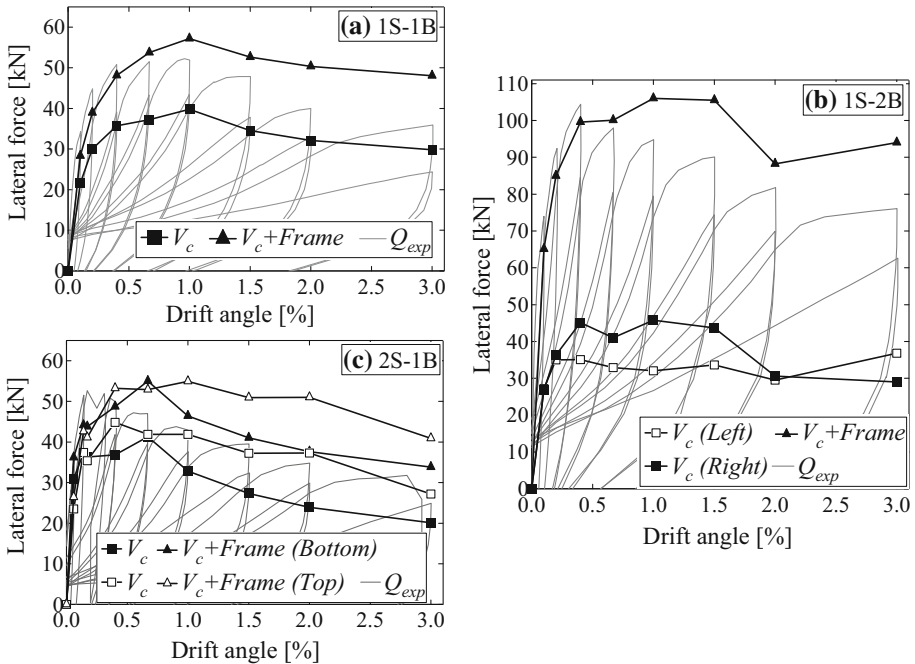


**Fig. 17** Evaluation of lateral load-drift angle relationships

In Specimen 1S-1B, the shear resistance estimated based on the strain data are in good agreement with the experimental lateral forces until  $R = 0.4\%$  rad. However, the estimations slightly exceeded the experimental values at a drift angle of  $1.0\%$  rad. when the specimen reached its capacity, possibly due to some CB units being neglected (at the right-top corner of the infill in Specimen 1S-1B, as shown in Fig. 7b), as noted above.

In Specimen 1S-2B, the estimated shear resistances were consistent with the experimental lateral forces until the maximum strength. However, the values based on strain data overestimated beyond the drift angle of 1.0% rad. because of significant damage to the infill walls.

In contrast, the estimated result of Specimen 2S-1B did not show good agreement with the experimental result. From this comparison and the identified equivalent diagonal strut shown in Fig. 15c, the equivalent diagonal strut identification method assuming a single strut formation in each infill by Jin et al. (2016) may not be applicable to multi-story infill, where independent multiple struts were likely to be formed, as illustrated in Fig. 16.

## 6 Conclusions

The current paper presented a series of experimental tests on Turkish RC moment-resisting frame models infilled with URM walls and investigated the in-plane behaviour of the infill walls based on a method to experimentally identify the diagonal strut formation proposed by Jin et al. (2016). The specimens considered in this study were one-story, two-bay frames and two-story, one-bay frames. The following major findings were obtained:

1. According to the experimental results, the seismic performance of the vertically stacked infill wall was lower than that of the horizontally stacked wall. The vertically stacked wall did not form a diagonal strut because of the rocking behaviour of each vertical block.
2. The maximum strength of Specimen 1S-2B was approximately twice that of Specimen 1S-1B. Alternatively, the maximum strength of Specimen 2S-1B, which exhibited the story collapse mechanism in the second story, was similar to that of Specimen 1S-1B.
3. Based on the above test results, the equivalent diagonal strut identification method by Jin et al. (2016) was applied to Specimens 1S-1B, 1S-2B and 2S-1B to investigate the lateral force resisting mechanisms. As a result, compressive struts were individually formed in both walls in Specimen 1S-2B; these struts were formed in a manner similar to the strut formed in Specimen 1S-1B. This result supports the effectiveness of analytical modelling based on a single strut for infill in multi-bay frames.
4. The identified compressive struts for Specimen 2S-1B implied that multiple struts might be formed, including a diagonal strut running through both stories. Although such behaviour might be attributed to the loading scheme adopted in this study, careful consideration is required to apply single-strut models to multi-story infilled frames.

The current paper focused only on the experimental behaviour, particularly the compression strut formation, of the masonry infilled RC frames. The experimental data should be investigated from theoretical and numerical perspectives in future studies.

**Acknowledgements** The project was funded by the CONCERT-Japan (Connecting and Coordinating European Research and Technology Development with Japan) project (Project leader: Professor P. Gülkan, currently at Middle East Technical University, Northern Cyprus Campus, Turkey, with support provided by the Scientific and Technological Research Council of Turkey under Project 113M557, Project leader in Japan: Professor Y. Nakano) under JST (Japan Science and Technology Agency). The authors are thankful to both agencies for their financial support.

## References

- American Concrete Institute (ACI) (2014) Building code requirements for structural concrete (ACI 318-14)
- Architectural Institute of Japan (AIJ) (2016) AIJ standard for lateral load-carrying capacity calculation of reinforced concrete structures (**in Japanese**)
- FEMA 306 (1998) Evaluation of earthquake damaged concrete and masonry wall buildings. Applied Technology Council (ATC-43 Project)
- Gere JM, Timoshenko S (1997) Mechanics of materials, 4th edn. PWS Publishing Company, Boston
- Gülkan P, Binici B, Sucuoğlu H, Taghipour A, Demirel O, Tanşer S, Güneş O, İsmail M, Fehling E, Nakano Y, Sanada Y, Choi H (2015) An innovative tie system for improving the monolithic behavior of masonry in-filled reinforced concrete frames (INFILTIE). In: 3rd Turkish national conference on earthquake engineering and seismology. 14–16 October 2015, Dokuz Eylül University, İzmir
- Hashemi A, Mosalam KM (2007) Seismic evaluation of reinforced concrete buildings including effects of masonry infill walls. In: PEER report 2007/100, Pacific Earthquake Engineering Research Center
- Holmes M (1961) Steel frames with brickwork and concrete infilling. Proc Inst Civil Eng 19:473–478. doi:[10.1680/iicep.1961.11305](https://doi.org/10.1680/iicep.1961.11305)
- Jin KW, Choi H, Nakano Y (2016) Experimental study on lateral strength evaluation of unreinforced masonry-infilled RC frame. Earthq Spectra 32:1725–1747. doi:[10.1193/00714EQS152M](https://doi.org/10.1193/00714EQS152M)
- Maidiawati Sanada Y, Konishi D, Tanjung J (2011) Seismic performance of nonstructural brick walls used in Indonesian R/C buildings. J Asian Archit Build Eng 10:203–210. doi:[10.3130/jaabe.10.203](https://doi.org/10.3130/jaabe.10.203)
- Mainstone RJ (1971) Summary of paper 7360: on the stiffness and strength of infilled frames. Proc Inst Civil Eng 49:230. doi:[10.1680/iicep.1971.6267](https://doi.org/10.1680/iicep.1971.6267)
- Stafford SB, Carter C (1969) A method of analysis for infill frames. Proc Inst Civil Eng 44:31–48. doi:[10.1680/iicep.1969.7290](https://doi.org/10.1680/iicep.1969.7290)
- Turgay T, Durmus MC, Binici B, Ozcebe G (2014) Evaluation of the predictive models for stiffness, strength, and deformation capacity of RC frames with masonry infill walls. J Struct Eng 140:06014003. doi:[10.1061/\(ASCE\)ST.1943-541X.0001069](https://doi.org/10.1061/(ASCE)ST.1943-541X.0001069)